# Faraday Discussions

## Accepted Manuscript


This manuscript will be presented and discussed at a forthcoming Faraday Discussion meeting. All delegates can contribute to the discussion which will be included in the final volume.

**Register now to attend!** Full details of all upcoming meetings: **http://rsc.li/fd-upcoming-meetings**


This is an *Accepted Manuscript*, which has been through the RSC Publishing peer review process and has been accepted for publication.

*Accepted Manuscripts* are published online shortly after acceptance, which is prior to technical editing, formatting and proof reading. This free service from RSC Publishing allows authors to make their results available to the community, in citable form, before publication of the edited article. This *Accepted Manuscript* will be replaced by the edited and formatted *Advance Article* as soon as this is available.

To cite this manuscript please use its permanent Digital Object Identifier (DOI®), which is identical for all formats of publication.

More information about *Accepted Manuscripts* can be found in the **Information for Authors**.

Please note that technical editing may introduce minor changes to the text and/or graphics contained in the manuscript submitted by the author(s) which may alter content, and that the standard **Terms & Conditions** and the **ethical guidelines** that apply to the journal are still applicable. In no event shall the RSC be held responsible for any errors or omissions in these *Accepted Manuscript* manuscripts or any consequences arising from the use of any information contained in them.

# Stability of carbonaceous dust analogues and glycine under UV irradiation and electron bombardment

**Belén Maté,* Isabel Tanarro, Miguel A. Moreno, Miguel Jiménez-Redondo, Rafael Escribano, and Víctor J. Herrero.**

Instituto de Estructura de la Materia, IEM-CSIC, Serrano 123, 28006 Madrid, Spain

*Corresponding author



## Abstract

The effect of UV photon (120-200 nm) and electron (2 keV) irradiation of analogues of interstellar carbonaceous dust and of glycine were investigated by means of IR spectroscopy. Films of hydrogenated amorphous carbon (HAC), taken as dust analogues, were found to be stable under UV photon and electron bombardment. High fluences of photons and electrons, of the order of $10^{19}$ $cm^{-2}$, were needed for a film depletion of a few per cent. UV photons were energetically more effective than electrons for depletion and led to a certain dehydrogenation of the HAC samples, whereas electrons, with a smaller penetration depth, led seemingly to a gradual erosion with no appreciable changes in the hydrocarbon structure. The rates of change observed may be relevant over the lifetime of a diffuse cloud, but cannot account for the rapid changes in hydrocarbon IR bands during the evolution of some proto-planetary nebulae.

Glycine samples under the same photon and electron fluxes decay at a much faster rate, but tend usually to an equilibrium value different from zero, especially at low temperatures. Reversible reactions re-forming glycine, or the build-up of less transparent products, could explain this behavior. $CO_2$ and methylamine were identified as UV photoproducts. Electron irradiation led to a gradual disappearance of the glycine layers, also with formation of $CO_2$. No other reaction products were clearly identified. The thicker glycine layers (a few hundred nm) were not wholly depleted, but a film of the order of the electron penetration depth (80 nm), was totally destroyed with an electron fluence of ~ $1 \cdot 10^{18}$ $cm^{-2}$. A 60 nm ice layer on top of glycine provided only partial shielding from the 2 keV electrons. From an energetic point of view, 2 keV electrons are less efficient than UV photons and, according to literature data, much less efficient than MeV protons for the destruction of glycine. The use of keV electrons to simulate effects of cosmic rays on analogues of interstellar grains should be taken with care, due to the low penetration depths of electrons in many samples of interest.

## 1 Introduction

Carbonaceous compounds, both solids and gas-phase molecules, are found in very diverse astronomical media[1]. They give the measure of the chemical complexity attainable in a given environment, and delimit the scenarios available for the chemical evolution towards life. A significant fraction of the elemental carbon is locked in large hydrocarbon structures forming small dust grains[2]. This carbonaceous dust, mostly formed in the last stages of evolution of C-rich stars, is the carrier of characteristic IR absorption bands revealing the presence of aliphatic, aromatic and olefinic functional groups in variable proportions.[3] Among the various candidate materials investigated as possible carriers of these bands, hydrogenated amorphous carbon (HAC) has led to the best agreement with the observations.[4] Carbonaceous grains are processed by H atoms, UV radiation, cosmic rays and interstellar shocks in their passage from asymptotic giant branch (AGB) stars to planetary nebulae (PN) and to the diffuse interstellar medium. In this environment, they could provide the source for clusters of polycyclic aromatic hydrocarbons (PAHs). Eventually, part of this material is incorporated into dense clouds and can end up as a component of planetary systems.[5] The mechanisms of HAC production and evolution in astronomical media are presently a subject of intensive investigation that requires not only detailed observations, but also laboratory work.[6-9]

Besides the large hydrocarbon structures just mentioned, many organic molecules, among them prebiotic species like sugars, amino acids, purines and pyrimidines have been identified in carbonaceous meteorites,[10] which are among the most primitive objects in the solar system. A rich organic inventory,[11] including the amino acid glycine,[12] has been found in comets, which are generally considered to contain some direct components from the prestellar core that gave rise to the solar nebula. A large number of organic compounds has also been recorded in observations of the interstellar medium (ISM),[13] with species of biological interest like precursors of sugars and molecules with peptidic bonds. Although the observation of glycine, the simplest amino acid, remains at best inconclusive,[14] its presence in the ISM is not unlikely since some of the molecules detected are of similar complexity. On the other hand, it is not clear whether complex and presumably fragile prestellar organic structures could survive the collapse of the protostellar core leading to the formation of a planetary system.[15] Establishing the conditions of survival of prebiotic molecules in various astronomical environments is nowadays a crucial issue for models of biogenesis.

The behavior of simple amino acids and specifically glycine in condensed phases relevant to astronomical media has drawn the attention of numerous research groups. The exchange between neutral and zwitterionic forms or the transitions between amorphous and crystalline phases as a function of temperature and chemical environment have been recently investigated in analogues of astronomical ices.[16,17] Likewise, the effects of bombarding these molecules with energetic ions[18-21], X-Rays[22,23] or UV photons[24-29] have been the subject of many studies. A global appraisal

of the different results on proton and photon irradiation is not straightforward because the experimental conditions are not always comparable and the interpretation of the data is complicated by the plurality of dissociation routes and secondary reactions.[30] Estimates based on the available data suggest that small amino acids could persist for tens or hundreds of Myr within the mantles of interstellar grains or under the surface of solar system bodies.

Energetic electrons are also known to be prevalent in astronomical media. They are present in the solar wind and in planetary magnetospheres and are also formed in the interaction of cosmic rays with matter. In interstellar grains, collision cascades induced by cosmic ray ions can lead to the production of secondary electrons with typical energies in the 0-10 keV range.[31] Although electron energies from a few eV to tens of eV are in principle the most adequate for chemical interactions, electrons with higher energies may be more efficient because they can penetrate deeper in the solids. Recent experiments by Barnett et al.[32] with electrons in the 100 eV-2keV interval have shown that the survival depth of organics in ices may be significantly lower than that expected from the electron penetration depth provided by current models based on Monte Carlo simulations.

The effects of electron irradiation on amino acids for astronomically relevant conditions have been less thoroughly studied than those of photons and ions. In some recent works, chemical routes for the electron stimulated formation of glycine[33,34] and even of dipeptides[35] have been explored at the surface or in the bulk of ices, but as far as we know, the survival of glycine under energetic electron bombardment has not yet been investigated. In this work we present the first results of a comparative study on the stability of HAC and glycine under bombardment by UV photons (120-200 nm) and 2 keV electrons. The investigation is based on IR spectroscopy of the samples of interest. The distinct features of photon and electron processing are discussed and compared to previous publications.

## 2. Experimental details

### 2.1. Plasma reactor.

Carbonaceous deposits were grown by plasma enhanced chemical vapor deposition (PECVD[36] in an inductively coupled RF discharge reactor. The reactor consists of a Pyrex tube, 30 cm length, 4 cm diameter, ended by two vacuum flanges (DIN 40KF). A 10 turns Cu coil placed externally around the central part of the tube, with a total length of 8 cm, was fed by a 13.56 MHz RF generator (Hüttinger PFG 300 RF + matchbox PFM 1500A) to produce the plasma, which was maintained at a constant power of 40 W during the deposition processes. One of the flanges of the reactor supports a piece holding an observation window and a narrow tube for gas input. This piece is easily

removed to introduce the deposition substrates. The second flange is connected through a vacuum cross piece to a regulating valve and a rotary pump, to the vacuum gauges (Pirani and absolute capacitance manometers); and to a quadrupole mass spectrometer (Balzers, Prisma Plus-QMG220) used as Residual Gas Analyzer (RGA). The RGA is placed in a differentially pumped vacuum chamber connected to the reactor through a ~ 50 μm diameter diaphragm. Typical pressures in the RGA chamber are five orders of magnitude lower than in the reactor.

The background pressure in the reactor was ~ $3 \cdot 10^{-3}$ mbar. For plasma generation, it was fed with a gas mixture of 40% $CH_4$ and 60% He through two fine needle valves, one for each gas, at 0.3 mbar total pressure. Gas residence time was estimated ~ 1 s. Two silicon substrates, 2.5 cm diameter, 1 mm thickness, were placed, in horizontal orientation, roughly in the central plane of symmetry of the reactor. One of the substrates was placed ~ 5 cm outside the coil in the direction of gas flow, and the other one in the central part of the coil. They were exposed approximately one hour to the depositing plasma. The deposited samples had a distinct appearance (see Fig. 1). Deposits formed outside the coil (labeled HAC1) were very uniform with shiny circular interference fringes. Deposits inside the coil (labeled HAC2) were dusty, black and irregular. The IR spectra of these samples, measured for the regions marked with circles in Fig. 1, will be discussed in the next section. A thickness of ~ 300 nm was estimated for the HAC1 samples from the interference fringes in the baseline of their IR spectra. The HAC deposits generated are stable enough to be handled and stored during months without appreciable alteration.

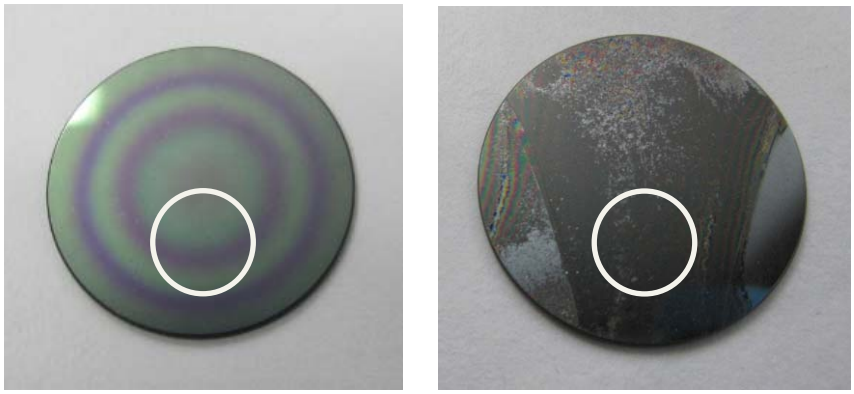

**Fig. 1:** Samples of hydrogenated amorphous carbon deposited on Si by PECVD in the inductively coupled RF discharge reactor. Left sample: HAC1, grown outside the inductive coil. Right sample: HAC2, grown inside the inductive coil (see text). The circles indicate the regions used for spectroscopic and/or processing experiments and for the deposition of glycine.

The RGA was used to identify the species produced during the discharge and to measure the dissociation degree of the $CH_4$ precursor. The method was similar to that used in previous works on film deposition by DC discharges.[37,38] $CH_4$ dissociation, determined from the evolution of the RGA signal at $m/q^+$ = 15 a.m.u, was ~ 70%. $H_2$ ($m/q^+$ = 2 a.m.u) and $C_2H_2$ ($m/q^+$ = 26 a.m.u) were identified as two of the main stable gas products. $C_2H_4$ and $C_2H_6$ are produced too, since clear increases at the $m/q^+$ = 27-30 a.m.u signals were observed, corresponding to the main peaks of the dissociation patterns of both species. $C_3H_x$ (x=4,6,8) formation could be also deduced from the signals at $m/q^+$ = 29, 37-41 a.m.u . Qualitative descriptions of the formation routes of $C_xH_y$ stable products and radicals in different $CH_4$ rich discharges, and of the main kinetic processes involved, can be found elsewhere.[39-42]

### 2.2 Cryogenic chamber.

The high vacuum cryogenic set up (Fig. 2) has been described elsewhere.[17,43] The stainless steel cylindrical chamber, with a residual pressure of $5 \cdot 10^{-8}$ mbar, contains a close cycle helium cryostat, whose cold finger holds an IR transparent Si window in close thermal contact. The temperature of the Si substrate can be varied between 14 K and 300 K with 1 K accuracy. The system is coupled to a Vertex70 FTIR spectrometer in normal incidence transmission configuration. A rotatable flange allows the orientation under vacuum of the Si substrate toward different chamber ports. In one position, it faces a sublimation mini-oven that is used to evaporate glycine. This oven, of our own design, was described in more detail previously.[17,44] The Si substrate can be turned to another window to record transmission spectra, and, in a third position, it faces the UV lamp or the electron gun, depending on the experiment. The spectra shown in this work were recorded with a Mercury Cadmium Telluride detector, adding between 50 and 300 scans, with 2 $cm^{-1}$ resolution.

The oven temperature for glycine sublimation was 140 ± 5 ºC. For water deposition on top of the glycine layer, $1 \cdot 10^{-5}$ mbar water vapor was admitted into the chamber through an independent line.

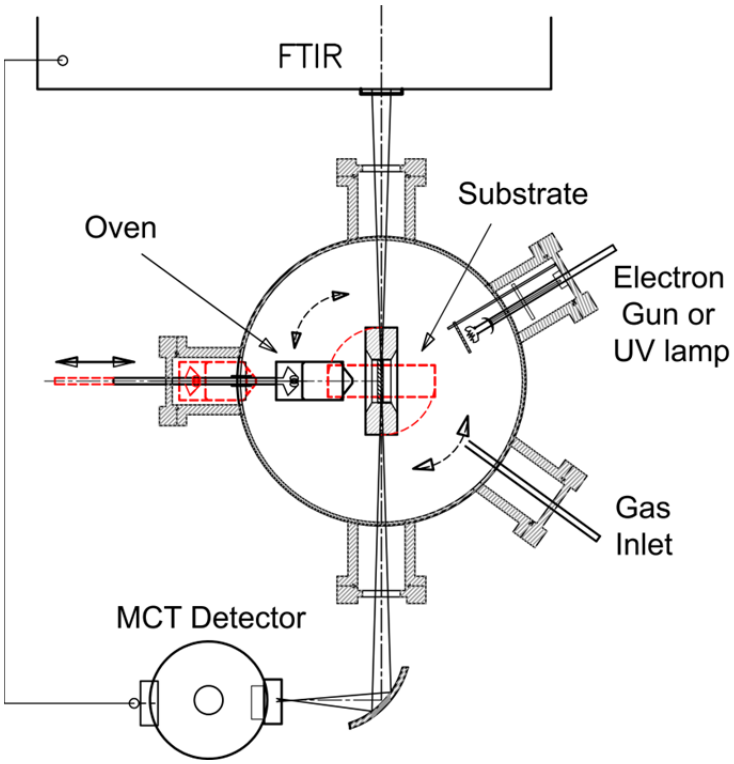


**Fig. 2.** Scheme of the cryogenic chamber. The UV lamp or electron gun can be interchanged to operate through the same window.

In a previous publication of our group, the amount of deposited glycine molecules was estimated from the IR spectrum via the absorption intensity in the 2000-800 $cm^{-1}$ frequency range, using a theoretical value for the absorption band strength in this spectral region.[17] However, it is difficult to estimate the errors in the absolute intensities. In the present investigation we have scaled our spectra to available literature data for samples where the thickness of glycine films was experimentally measured. In particular, we adopted the values of ten Kate et al.[26] for vapor deposited crystalline glycine at room temperature and that of Gerakines et al.[20] for amorphous glycine at 20 K. The thickness of our layers varied between 80 and 900 nm, depending on the experiment.

### 2.3. UV lamp.

The source for UV irradiation was a HAMAMATSU L10706, UV D2 lamp. The lamp is provided with a flexible pipe that allows placing its $MgF_2$ window at 30 mm from the sample, inside the vacuum chamber. The UV beam has a diameter of 13 mm at the output window and a divergence of 7.5 degrees. The integrated emission flux in the 120 nm-200 nm wavelength range at 30 mm from the lamp window is $4 \cdot 10^{14}$ photons $cm^{-2}$ $s^{-1}$, as calculated for our particular configuration from the data provided by the manufacturer. The spectral profile of the lamp, also provided by the manufacturer, has a maximum at 155-165 nm, about 7 times more intense than the average emission of the

rest of the wavelength interval. We have taken an approximate average energy of 7.6 eV for our photons.

### 2.4. Electron gun.

The electron source used for sample processing was built in our laboratory. It is based on the design used previously for electron-seed plasma ignition in our DC discharge reactors at low pressures.[42] It consists of a tungsten filament, 130 μm diameter, ~ 20 mm long, curled to form a small spiral of about 10 mm length. The filament turns white bright and emits electrons efficiently with a current of about 2.2 A. To extract the electrons and direct them to the target, which in our case is electrically connected to ground, the filament can be negatively biased up to -2.5 kV, and a grounded grid is placed between the filament and the target, at 10 mm from the filament. The extracting grid is circular, with a 20 mm diameter, made of a mesh with a separation of ~ 1 mm between parallel wires. The accelerated electrons going through the grid reach the target with an energy determined by the applied potential. The size of the electron beam is controlled by the size of the grid. The whole system is placed inside the vacuum chamber, and the accelerating grid is located 35 mm away from the target. In our experiments, the targets are the Si substrates with the HAC or glycine samples.

The flux of electrons reaching the samples was calibrated by replacing the Si substrate in the cryostat finger by an electrode of the same size as the sample holder (a copper disk, 1 cm diameter), placed exactly at the same place as the samples. The current from the electron gun reaching the calibration electrode was measured by means of a microamperimeter. We found that the electron flux reaching the target was proportional to the emission current and did not depend strongly on the accelerating potential. For the irradiation experiments presented in this work we have used a flux of $2.66 \cdot 10^{14}$ electrons $cm^{-2}$ $s^{-1}$, with an energy of 2.0 keV. This electron flux corresponds to an emission current of 4.6 mA (between the filament and the grid) and an electron current of 42 $\mu A/cm^2$ at the target.

## 3. Results and discussion

### 3.1. Carbonaceus deposits.

Fig. 3 shows the spectra of two of the carbonaceous deposits described in the previous section. Different deposits grown in analog conditions had very repetitive spectra. Note that the IR absorption by the HAC2 sample is much smaller. Both spectra exhibit the characteristic features of HAC materials, but with different proportions. The following assignments are taken from refs. 7 and 9. In the region around 2900 $cm^{-1}$ (~ 3.4 μm) the maximum in the HAC1 spectrum corresponds to the peak at 2959 $cm^{-1}$, which is assigned to the asymmetric stretching of aliphatic $CH_3$ groups, whereas in the HAC2 spectrum the maximum is found at 2929 $cm^{-1}$ and is due to asymmetric stretching vibrations of the aliphatic $CH_2$ group. The two peaks at 1450 and 1370 $cm^{-1}$ are

attributed to deformation modes of $CH_2$ and $CH_3$ respectively. Again in this case the $CH_2/CH_3$ intensity ratio is larger for HAC2. The broad band in the 1600 $cm^{-1}$ region is much stronger (in relative value) for HAC2, with a peak at ~ 1615 $cm^{-1}$ attributed to aromatic and olefinic C=C stretching modes. Features below 1000 $cm^{-1}$ are also assigned to aromatic and olefinic vibrations.

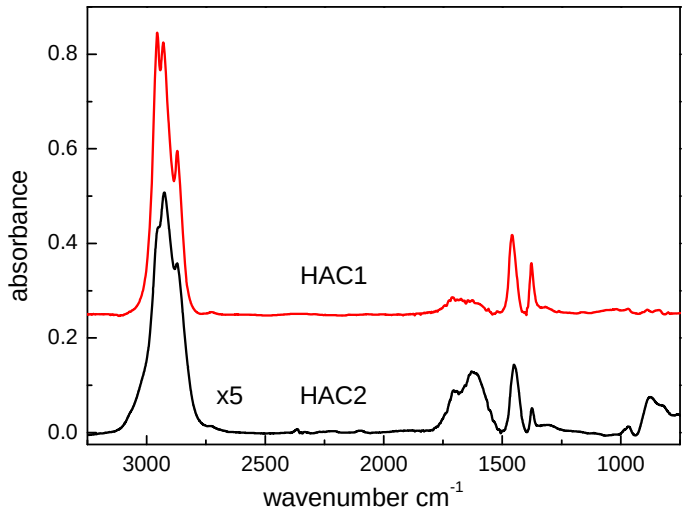


**Fig. 3**. IR spectra of the carbonaceous deposits shown in Fig. 1. The spectrum of the HAC2 sample has been magnified by a factor of 5. The spectrum of HAC1 is offset in the absorbance scale to facilitate the comparison.

The analysis of the spectra shows that both samples have aliphatic chains, but the deposit generated inside the coil of the plasma reactor, subjected to a more intensive attack by the ions and radicals in the discharge, has smaller hydrogen content and higher proportion of aromatic and olefinic components. This result is in agreement with intuitive expectations based on the more graphitic appearance of the HAC2 layer, as shown in Fig. 1. Dartois et al.[7] have produced HAC samples of variable composition by UV photolysis of different hydrocarbon precursors. Their HAC samples generated from methane or ethane produce spectra that resemble that of HAC1 in Fig. 3. On the other hand, their HAC from a xylene precursor yields a spectrum in which the 3.4 μm (~2900 $cm^{-1}$) band structure is close to that observed in our HAC2 spectrum. A similar 3.4 μm band, with a maximum in the central peak, is also seen in the IR spectra of HACs obtained by other groups with different methods. Mennella et al.[6] used hydrogenation of nano-sized carbon grains by a flux of H atoms; Kovačević et al.[8] employed a RF discharge of $C_2H_2$ and Ar; and Gadallah et al.[9] used ablation of graphite in hydrogen atmosphere. The band profiles from these and other laboratory samples[4] give a good match to the shape of the 3.4 μm band observed in the diffuse ISM.[2,4,7] The ubiquity of this band shape suggests a very stable underlying structure.

In the following, we report on the distinct effects of UV light and electron bombardment on HAC1 at room temperature. The sample was irradiated during 24 hours with a flux of $4 \cdot 10^{14}$ UV photons $cm^{-2}$ $s^{-1}$ from a deuterium lamp (~ 160 nm), which corresponds to a dose of $2.63 \cdot 10^{20}$ eV $cm^{-2}$, assuming an energy of 7.6 eV for the photons. The effects of this irradiation can be seen in panel a) of Fig. 4, where a difference spectrum (irradiated sample-non irradiated sample) of the 3.4 µm band is displayed. A very small decrease in peak intensity (~2%) can be seen. The peaks in the difference spectrum are slightly displaced with respect to the HAC1 peaks because the decrease is more pronounced toward the high frequency end of the band, corresponding to the $CH_3$ asymmetric stretching, and less so at the central peak ($CH_2$ stretching). This behavior hints at an evolution towards the 3.4 µm band profile of HAC2 and thus to a loss of hydrogen. In order to visualize this effect we have represented in panel c) of the same figure the effect of multiplying by 20 the absorbance decrease of panel a). For the wavelength region below 2000 $cm^{-1}$, where the bands are much weaker, we could not derive reliable difference spectra.

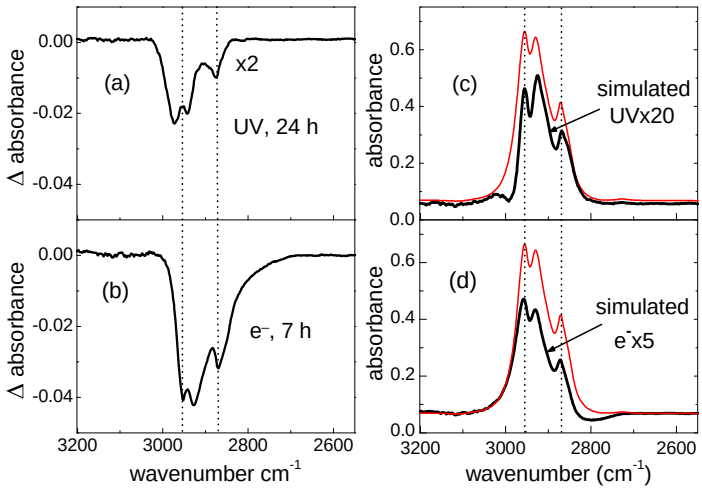


**Fig. 4.** Evolution of the 3.4 µm band of HAC1. Panel a) Difference spectrum (irradiated – non-irradiated) of the UV processed HAC1 sample (dose: $2.63 \cdot 10^{20}$ eV/$cm^2$). Panel b) Id. of the HAC1 sample processed with electrons (dose: $1.34 \cdot 10^{22}$ eV/$cm^2$). Panel c) Thin red line: HAC1 spectrum; thick black line: simulated spectrum after multiplying by 20 the absorbance decrease of panel a). Panel d) Thin red line: HAC1 spectrum; black solid line: simulated spectrum after multiplying by 5 the absorbance decrease of panel b).

If we take an estimate of $3 \cdot 10^8$ eV $cm^{-2}$ $s^{-1}$ for the UV flux in a diffuse cloud,[9] our irradiation time corresponds to approximately $2.8 \cdot 10^4$ years. Over this time, the HAC1 material should be essentially stable in the diffuse ISM, with only a slight tendency to lose hydrogen atoms and form longer chains.

Much larger irradiation doses were used by Gadallah et al.[9] in their study of the effect of 160 nm UV photons from a deuterium lamp on HAC samples. The IR spectra of the unprocessed deposits of Gadallah et al. are closer to those of HAC2 in the present work. After a dose of $1 \cdot 10^{23}$ eV $cm^{-2}$, which corresponds to one third of the estimated lifetime of a diffuse cloud,[9] these authors observed a marked decrease of all aliphatic features (more than 80% at the maximum of the 3.4 μm band). The characteristic profile of the band, with a maximum in the central peak, was maintained, further corroborating the stability of this structure. Our experimental results suggest that the hydrogen-richer HAC1 material will also evolve toward this structure with sufficient UV irradiation. Gadallah et al. also found an increase in some of the aromatic bands and concluded that UV irradiation could explain the evolution of HAC toward PAHs during the lifetime of a diffuse cloud. Our measurements were not sensitive enough to variations in the aromatic features. However, the evolution rate observed both by Gadallah et al. and by us is too slow to justify the appearance and evolution of aliphatic and aromatic features in proto-planetary nebulae on time scales as short as a few hundred years.[3]

The effects of electron bombardment on HAC1 are shown in panel b) of Fig. 4. In this case, the sample was irradiated during seven hours with a $2.63 \cdot 10^{14}$ $cm^{-2}$ $s^{-1}$ flux of 2 keV electrons. The total processing dose was $1.34 \cdot 10^{22}$ eV $cm^{-2}$. After this dose, the depletion in the peaks of the 3.4 μm band was about ~ 8%. A comparison with the previous measurements shows that, although the depletion efficiency per photon is lower than that per electron, the energetic efficiency is much higher for photon irradiation. The difference spectrum for the electron irradiated sample does not show a preferential decrease of $CH_3$ bands, as compared with $CH_2$ bands. To make this point more clear we have represented in Fig. 4.d) the simulated HAC1 spectrum after multiplying by 5 the absorbance decrease of panel b). The hints of dehydrogenation reflected in the growth of the $CH_2/CH_3$ ratio, commented on for the UV case, are not found here. It seems that electron bombardment erodes gradually the film rather than transforming it.

The penetration of electrons in solids is determined by a complex series of energy loss processes involving the production of UV and X-Ray bremsstrahlung, the generation of secondary electrons, ions and other reactive species, and ultimately the interaction with phonons and the dissipation of thermal energy. Penetration depths are usually estimated with the help of Monte Carlo simulations. Predictions with the CASINO code[45] for 2 keV electrons impinging on hydrogenated carbon yield penetration depths between 90 and 120 nm, depending on the assumed density and hydrogen content. For our estimated film thickness of 300 nm, all electrons will be stopped within the first third of the HAC1 deposit and will not interact at first with the whole sample. The deeper part of the HAC1 deposit will be reached by electrons only after the depletion of the outer layers. Although we do not know the detailed structure of the HAC1 films or their cross sections for absorption of UV photons, it is likely that the films are optically thin for the photons used in our experiments. In contrast with the electron bombardment, the whole film would thus be available for the photons since the beginning of irradiation.

### 3.2.Glycine

Fig. 5 shows the spectra of glycine films deposited on a cold (20 K) Si substrate and then irradiated with UV photons or electrons. Appreciable differences are found in the spectra of the differently processed samples. The spectra show that the deposited films, 600 and 900 nm thick respectively, are amorphous solids, where the glycine molecules are predominantly in a zwitterionic form[17] as shown by the small intensity of the characteristic neutral bands,[17] at 1730 and 1240 $cm^{-1}$. Spectra of thinner films (< 400 nm) deposited at this temperature have a significant component of the neutral form. The low temperature transformation from neutral to zwitterionic with growing thickness is not well understood at present and will be studied in more detail in further works.

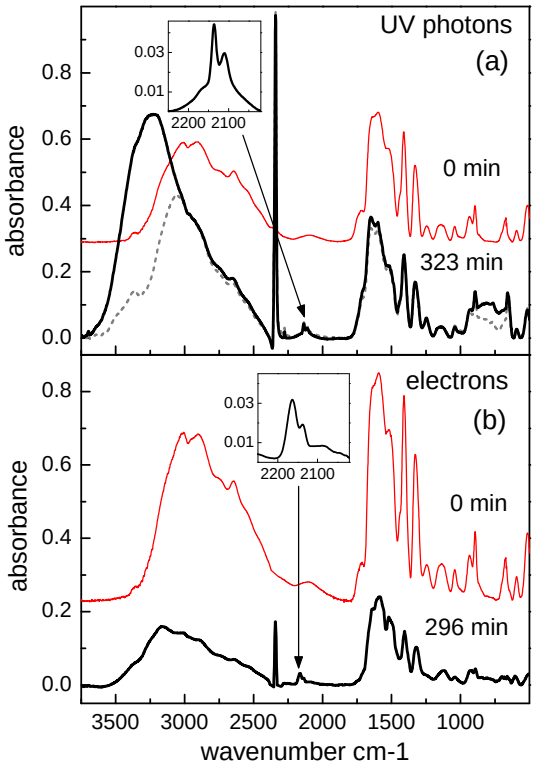


**Fig. 5**: IR spectra of amorphous glycine deposited at 20 K. Top: 600 nm thick deposit before (red) and after 323 min processing by UV photons. Bottom: 900 nm thick sample, before (red) and after 296 min bombardment with 2.0 keV electrons.

In the UV irradiated glycine film (Fig. 5.a) large bands of water (3500-3000 $cm^{-1}$) and $CO_2$ (2341 $cm^{-1}$) grow during the experiment. These bands are attributed to deposition of background molecules. The band intensities correspond to layers of ~200 nm water and ~60 nm $CO_2$ that are consistent with the expectations for the five hour experiment. Part of the $CO_2$ peak is surely due to glycine decomposition. Much smaller peaks are observed at 2136 $cm^{-1}$ (CO stretch) and at 2110 $cm^{-1}$ (see inset in panel a) of Fig. 5). This latter peak could be due to chain oxides of the $C_xO_y$ type.[46] Other peaks of

photolysis products appear on top of the glycine bands between 1780 and 1450 $cm^{-1}$ and will be commented on below. The small amount of neutral glycine present in the initial deposit does not disappear upon UV irradiation, as attested by the peak at 1240 $cm^{-1}$. The subtraction of the water contribution to the spectrum is also shown with a dotted line.

In the glycine deposit bombarded with electrons, no water is formed on top after a five hour experiment with the same chamber conditions. A peak appears at 2341 $cm^{-1}$, attributed to $CO_2$, but the absence of a water layer, and the fact that this peak is shifted by a few $cm^{-1}$ with respect to that of pure $CO_2$, suggest that it corresponds to $CO_2$ surrounded by other molecules within the bulk of the sample.[47] It is most probably a product of glycine decomposition. Smaller peaks appear too at 2136 $cm^{-1}$ (CO stretch) and at 2164 $cm^{-1}$, which could be due to $OCN^-$.[48] In the region between 1750 and 1000 $cm^{-1}$ the two bands of the neutral form, at 1730 and 1240 $cm^{-1}$, disappear almost totally but, otherwise, no significant changes are observed in the band profile. A most notable feature of this experiment was the gradual temperature increase in the sample and substrate during the intense electron irradiation. In the first four hours of the experiment the temperature increased from 20 to 76 K and then stabilized.

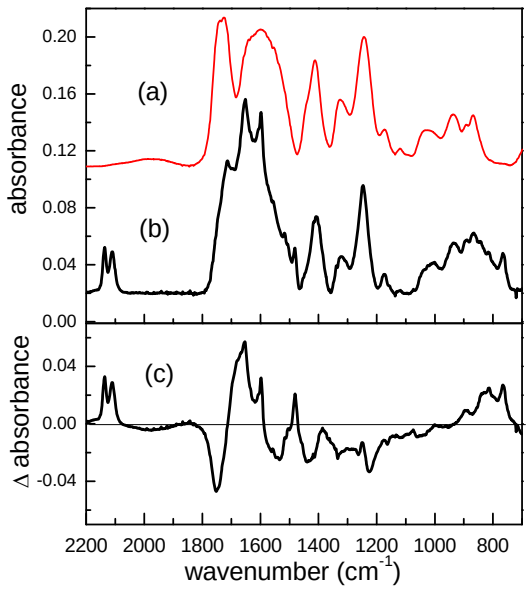


**Fig. 6.** IR spectrum of a thin amorphous glycine layer deposited at 20 K, a) before and b) after 280 min irradiation with UV photons. c) Difference spectrum: b) –a).

In an attempt to identify products of the photolysis of glycine in the 1780-1440 $cm^{-1}$ spectral range, we intensified the changes by performing an experiment on a thinner layer (150 nm) deposited at 20 K. The results are shown in Fig. 6. In the upper trace of the top panel, corresponding to the spectrum of the unprocessed sample, the two bands of neutral glycine (1730 and 1240 $cm^{-1}$) characteristic of amorphous thin films are

clearly visible. The lower trace of the upper panel, corresponding to the irradiated sample, shows a number of new peaks on top of glycine bands. In the lower panel, the difference spectrum (irradiated-non irradiated) is shown.

Tentative assignments of the positive peaks in the difference spectrum of Fig. 6 are listed in Table 1. The peaks at 2136 and 2110 $cm^{-1}$ were commented on above. The peaks at 1650, 1598 and 1482 $cm^{-1}$ are assigned to methyilamonium ions and to methylamine. The $\nu_9$ $NH_2$ wagging vibration of methylamine has been variously attributed to the 895 $cm^{-1}$ peak[49] or to the 819 $cm^{-1}$ peak,[33] not included in the table, but also present within the positive band at low frequency. The production of methylamine, and the likely presence of $CO_2$ (see above), point at decarboxylation as one of the main mechanisms of destruction of glycine upon UV irradiation, as already noted in previous works.[24,26]

**Table 1**. New infrared band positions ($cm^{-1}$) of the processed sample at 20 K after irradiation with UV photons.

| Wavenumber (cm-1) | molecule | Assignment |
|---|---|---|
| 2136 | CO | $\nu_1$ stretch CO |
| 2110 | CxOy oxides | $\nu_1$ stretch CO, ref. 46 |
| 1650 | $CH_3$ $NH_3^+$ | $\nu_9$, asymmetric bending $NH_3$, ref 49 |
| 1598 | $CH_3NH_2$ | $\nu_4$ scissor $NH_2$, ref 33 |
| 1482 | $CH_3NH_2$ | $\nu_{12}$ antisymm. def. $CH_3$, ref 33 |

Processing experiments were also carried out with the same electron and photon fluxes, on ~500 nm thick glycine layers deposited at 300 K. At this temperature, crystalline β glycine was obtained.[19,21,26] The decay of these samples was much faster (see below), and no evidence of new products was seen in the spectra, which was not unexpected, since volatile species are not retained at this temperature. With electron processing, a 570 nm film was eliminated after 77 min, leaving a persistent residue, insoluble in water, with a broad absorption band between 1850 and 1000 $cm^{-1}$.

The rate of disappearance of glycine was traced by monitoring the integrated intensity of its 1400 $cm^{-1}$ COO stretching band. The results are shown in Fig. 7.

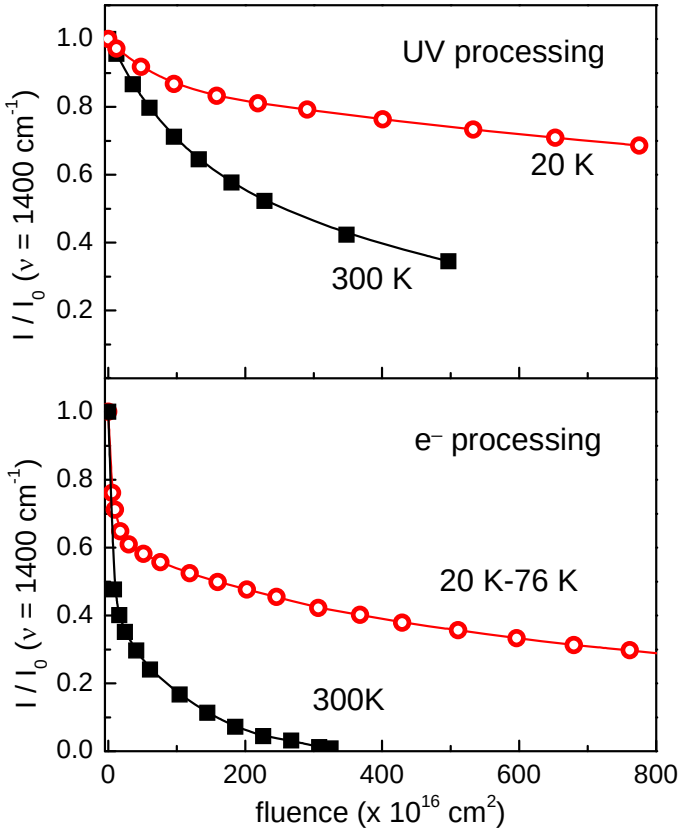


**Fig. 7.** Decay of the normalized intensity of the 1400 $cm^{-1}$ feature of glycine versus fluence of processing agent. Upper panel: UV photons (160 nm, 7.6 eV); circles: 600 nm layer, 20 K; squares: 460 nm layer, 300 K. Lower panel: electrons (2 keV); circles: 900 nm, 20-76 K; squares: 570 nm, 300 K.

At a given fluence, 2 keV electrons are always more efficient than 160 nm (7.6 eV) photons for the decomposition of glycine but, as in the case of carbonaceous films discussed above, the energetic efficiency is much higher for the photons. The process of interaction of photons and electrons with glycine is also expected to be very different. Estimates of the cross section for UV absorption by glycine solid samples have been given by ten Kate et al.[26] For the 120-180 nm wavelength range, which is close to the 120-200 nm range of our deuterium lamp, these authors provided values of the dissociation cross section of ~ $2 \cdot 10^{-19}$ $cm^{-2}$/molecule. Their experiments were carried out on crystalline β glycine, but we will assume that the corresponding value for our amorphous low temperature glycine is of the same order. For this value of the cross sections, all our glycine films are optically thin with respect to the UV photons.

In principle, first order kinetics could be expected for the photolysis of glycine, but this is not what is found in our experiments. After a relatively fast decay at the start, the curves in the upper panel of Fig. 7 stabilize and tend asymptotically toward values markedly different from zero. For the 20 K experiment, the total amount of glycine

destroyed for a photon fluence of $8 \cdot 10^{18}$ photons $cm^{-2}$ is only 30%. Deviations from the first order kinetics law have also been observed by other authors in experiments of amino acid photolysis[29] or proton processing.[19] Gerakines et al.[19] suggested that an equilibrium value different from zero could be due to reversible processes within the sample. An alternative explanation would be the gradual shielding of the sample by a photolysis product less transparent to the UV photons.[25,50] The deposition of background water and $CO_2$ on the sample during the 20 K UV irradiation experiment is not expected to perturb the photolysis of glycine, since the thin layers of these two molecules should be essentially transparent.

The hypothesis of reversible reactions could also explain the slower decay rate at low temperatures. The photolysis of glycine is expected to produce small volatile products[30] and, at low temperatures, these products would remain in the sample and be available for reactions leading back to glycine. Our experiments cannot decide on the cause of the slow decay, but in any case the observed behavior renders questionable the derivation of a meaningful half-life time from these measurements.

In the electron bombardment experiments (lower panel of Fig. 7) the situation is different. Estimates based on the CASINO code indicate that the penetration depth of 2 keV electrons in the glycine solid should be ~ 80 nm. The bulk of the glycine samples would thus be accessed only gradually after a layer by layer removal of the outer material. As a consequence, water and $CO_2$ cannot deposit since a fresh surface is continually being created by the electrons. It seems also clear that a significant amount of the energy delivered by the electrons is dissipated as heat, as shown by the temperature increase of the substrate in the course of the measurements. An experiment with a lower electron flux ($5 \cdot 10^{13}$ electrons $cm^{-2}$ $s^{-1}$) was carried out to check the possible influence of the raising temperature on the observed depletion rate. In this case, the temperature stabilized at 35 K and the same decay rate was observed. The slower decay in the low temperature experiments could also be due to reversible reactions with products of glycine decomposition that do not evaporate for temperatures below 80 K. Gerakines et al.[19] have recently reported the decay at 15 K of a 900 nm thick glycine sample irradiated with 0.8 MeV protons. They observed a 50% decrease of the initial intensity for a fluence of $4 \cdot 10^{14}$ protons $cm^{-2}$, as compared with $1.6 \cdot 10^{18}$ electrons $cm^{-2}$ in the present experiment (see Fig. 7). The electrons will leave most of their energy in the "opaque" solid, whereas the 0.8 MeV protons will only leave 4.2 eV (~0.5% of their energy) in the sample that has a stopping power of 4.67 eV/μm.[19] It is clear that MeV protons are much more efficient than keV electrons for the destruction of glycine, at least in samples of hundreds of nm.

### 3.3 Water ice on glycine

In the final part of our work we have investigated the electron bombardment of a thin film of glycine and the shielding effect of a water ice layer on top of it. First, an amorphous glycine deposit of 80 nm thickness was prepared at 20 K on a cold substrate. In this case, the glycine was deposited on a Si window previously covered by a

hydrogenated amorphous (HAC1) film. As discussed earlier, HAC is a likely component of interstellar dust. The glycine sample was then bombarded with the same electron flux used in the previous experiments ($2.66 \cdot 10^{14}$ electrons $cm^{-2}$ $s^{-1}$), and the integrated intensity of the 1400 $cm^{-1}$ band was employed to follow the evolution of glycine during electron irradiation. The results of the measurements are shown in Fig. 8 (squares). Note the heating of the samples upon electron bombardment commented on previously. The selected film thickness is of the order of the penetration length predicted by the CASINO software and the whole film is subjected to the effects of the electrons since the beginning of the process. After a sharp decay of about 15%, the band intensity shows a plateau associated to the transformation from the neutral to the zwitterionic form of the amino acid. When the transformation is complete, the decay continues until the total disappearance of the glycine film. A 50% decay is achieved with a fluence of ~ $3 \cdot 10^{17}$ electrons $cm^{-2}$, much lower than the corresponding value ($1.6 \cdot 10^{18}$ electrons $cm^{-2}$) for the 900 nm film studied previously. The difference is consistent with the gradual penetration of electrons in the thicker film commented on above.

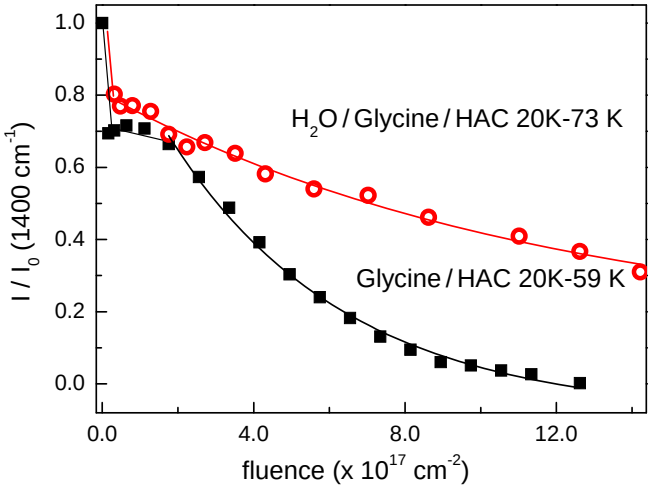


**Fig. 8.** Decay of the normalized intensity of the 1400 $cm^{-1}$ feature of glycine versus time of electron irradiation for glycine uncovered (squares) and covered with a 60 nm $H_2O$ layer (circles).

To study the effect of ice shielding, the experiment was repeated after growing a 60 nm water ice layer on an 80 nm glycine film deposited on HAC1 at 20 K. This ice thickness is realistic for interstellar grain mantels. The results of the electron irradiation experiment are shown in Fig. 8 (circles). Glycine is still destroyed by the electrons, but now at a slower pace. A 50% fall in intensity requires now roughly twice the electron fluence of the unshielded film. Simulations with the CASINO code showed that for vapor deposited water ice, with an assumed density of 0.67 g $cm^{-3}$, the electron penetration depth should be close to 200 nm. The predictions of the CASINO model

further show that a significant number of electrons pierce the 60 nm water ice shield and deposit their energy within the first 30 nm of the glycine film. The relatively high permeability of ice to the penetration of electrons in the keV range was recently stressed by Barnet et al.[32] Further work is in progress to better quantify ice shielding effects.

In Fig. 9 we present a final comparison of the energetic efficiency of MeV protons, vacuum UV photons and keV electrons for the destruction of glycine in cold (< 25 K) samples using data from this work and previous publications. This figure displays the decay of the 1400 $cm^{-1}$ band as a function of the energy irradiated per glycine molecule. All samples chosen for this comparison are optically thin for the respective processing agents. The highest efficiency corresponds to protons and the lowest to electrons. The photon results, from different experiments including solid layers and matrices, show certain dispersion, but lie between those of protons and electrons. Note that the plateau in the electron curve corresponds to the neutral to zwitterionic transformation commented on above (Fig. 8). The higher efficiency of protons and photons is even more marked if the actual energy deposited by the three processing agents in the samples is considered.

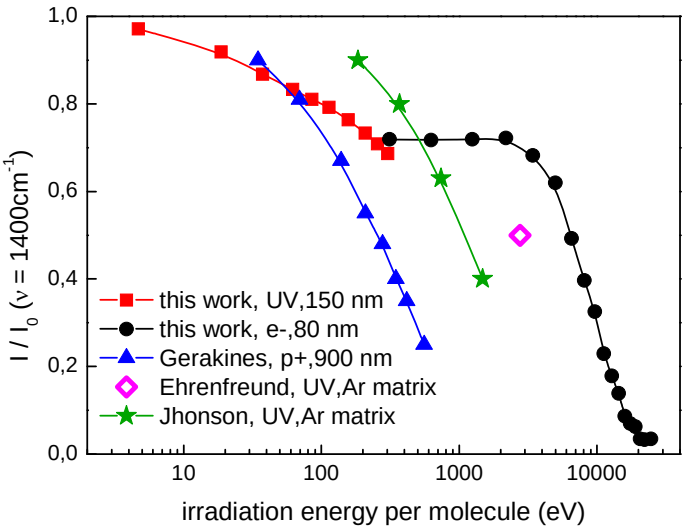


**Fig 9**. Evolution of glycine 1400 $cm^{-1}$ band as function of the energy irradiated on the sample normalized to the number of glycine molecules in the sample. This work: experiments (squares and circles). Literature data: triangles, from ref. 19; stars, from ref 29; rhombus, from ref. 24. For the Ar matrices, the dilution factor has been considered.

Kaiser et al. have suggested[33,35] that the effects of cosmic ray ions with energies in the MeV range could be mimicked with a bombardment of electrons in the keV range. This process should deposit a comparable amount of energy into the sample and would reproduce the secondary electron cascades expected for cosmic ray interaction. However, the comparison of the present experiments with the results of Gerakines et

al.[19] does not support this assumption. It seems that electron cascades produced by cosmic rays within the bulk of solids are much more efficient for inducing chemical transformations than electron bombardment from the outside.

## Conclusions

Hydrogenated amorphous carbon deposits are relatively stable under UV photon and electron bombardment. Decays of just a few percent in the HAC IR intensity are observed for comparatively high fluences (~ $10^{19}$ $cm^{-2}$). UV photons (160 nm, 7.6 eV) are found to induce a certain dehydrogenation of the hydrocarbon structure, probably increasing chain length. Bombardment with 2 keV electrons is energetically less efficient for depletion. It does not seem to change the structure of the hydrocarbons, but produces a layer by layer erosion of the films. Extrapolation of photon fluxes to the conditions of the diffuse interstellar medium reveals that the measured rates are significant as compared with the lifetime of a diffuse cloud, but too slow to justify the fast variation of IR hydrocarbon bands often observed in the evolution of proto-planetary nebulae.

Glycine samples subjected to comparable UV and electron fluxes are much more labile and decay at much faster rates. However, in many cases, especially in the experiments carried out at low temperatures (20-70 K), the glycine concentration tends to an equilibrium value different from zero. This equilibrium concentration could be determined by the build-up of less UV transparent products or by reversible reactions. At low temperatures, the largely volatile products of decomposition would remain in the sample and be available for reforming glycine. In accordance with previous works, decarboxylation, with production of $CO_2$ and methylamine, is found to be a main route of glycine UV photolysis. CO and possibly $C_xO_y$ oxides are also found among the reaction products.

Electron bombardment of glycine seems to proceed in a much more indiscriminate way affecting especially the outer layers, which are gradually depleted before electrons access the bulk of the sample. $CO_2$, CO and possibly $OCN^-$ are identified in the low temperature irradiated samples. A water ice layer of 60 nm, comparable in thickness to interstellar grain mantels, is found to shield glycine only partially from electron bombardment. A comparison of our results with previous literature works indicates that, from the energetic point of view, MeV protons are more efficient than UV photons, and these, more efficient than keV electrons for the destruction of glycine. The use of keV electrons to simulate the interaction of cosmic rays with matter should be taken with care, since the effects of electrons are extremely dependent on the sample thickness in the tens of nm range.

## Acknowledgements

We are indebted to Yamilet Rodríguez-Lazcano for her help with part of the measurements to J. A. Martín Gago for advice on the construction of the electron gun, and to Ó Gálvez for helpful discussions. This work was funded by the MCINN of Spain under grants FIS2010-16455 and CDS2009-00038. M. Jiménez-Redondo acknowledges also funding from the FPI program of the MICINN.

## References

1 A. G. G. M. Tielens, *Rev. Mod. Phys.* 2013, **85**, 1021

2 J. E. Chiar, A. G. G. M. Tielens, A. J. Adamson, and A. Ricca, *Astrophys. J.*, 2013, **770**, 78

3 S. Kwok, in *The Molecular Universe*, J. Cernicharo and R. Bachiller ed, IAU Symposium 280, Cambridge University Press, 2011, p 203,

4 Y. J. Pendelton and L. J. Allamandola, *Astrophys. J.* 2002, **138**, 75.

5 G. M. Muñoz Caro and E. Dartois, *Chem. Soc. Rev*, 2013, **42**, 2173

6 V. Mennella, J. R. Brucato, L. Collangeli and M. E. Palumbo, *Astrophys. J.* 2002, **569**, 531.

7 E. Dartois, G. M. Muñoz Caro, D. Deboffle, G. Montagnac, and L. D´Hendecourt, *Astron. Astrophys.*, 2005, **432**, 895.

8 E. Kovačević, I. Stefanović, J. Berndt, Y. J. Pendelton, and J. Winter, *Astrophys. J.* 2005, **623**, 242.

9 K. A. K. Gadallah, H. Mutschke, and C. Jäger, *Astron. Astrophys.*, 2012, **544,** A107

10 O. Botha and J. L. Bada, *Surv. Geophys.* 2002, **23**, 411.

11 M. J. Mumma and S. B. Charnley, *Ann. Rev. Astron. Astrophys*, 2011, **47**, 471.

12 J. E. Elsila, D. P. Glavin, and J. P. Dworkin, *Meteor. Planet. Sci.*, 2009, **44**, 1323.

13 E. Herbst and E. F. van Dishoeck, *Ann. Rev. Astron. Astrophys.*, 2009, **47**, 427.

14 L. E. Snyder, F. J. Lovas, J. M. Hollis, D. N. Friedel, P. R. Jewell, A. Remijan, V. V. Ilyushin, E. A. Alekseev and S. F. Dyubko, *Astrophys J*, 2005, **619**, 914.

15 P. Ehrenfreund and M. A. Sephton, *Faraday Discuss.*, 2006, **133**, 277.

16 A. Gómez-Zavaglia and R. Fausto, *Phys. Chem. Chem. Phys.*, 2003, 5, 3054.

17 B. Maté, Y. Rodríguez-Lazcano, O. Gálvez, I. Tanarro, and R. Escribano, *Phys. Chem. Chem. Phys.*, 2011, **13**, 12668

18 W. Huang, Z. Yu, and Y. Zhang, *Chem. Phys.*1998, **237**, 223

19 P. A. Gerakines, R. L. Hudson, M. H. Moore and J-L Bell, *Icarus*, 2012, **220**, 647.

20 P. A. Gerakines and R. L. Hudson, *Astrobiology*, 2013, **13**, 647.

21 S. Pilling, L. A. V. Mendes, V. Bordalo, C. F. M. Guaman, C. R. Ponciano, and E. F. da Silveira, *Astrobiology*, 2013, **13**, 79

22 S. Pilling, D. P.P. Andrade, E. M. do Nascimento, R. R. T. Marinho, H. M. Boechat-Roberty, L. H. de Coutinho, G. G. B. de Souza, R. B. de Castilho, R. l. Cavasso-Filho, A. F. Lago, and A. n. de Brito, *Mon. Not. R. Astron. Soc.*, 2011, 411, 2614.

23 A. Pernet, J. Pilmé, F. Pauzat, Y. Ellinger, F. Sirotti, M. Silly, Ph. Parent, and C. Laffon, *Astron. Astrophys.*,2013, **552**, A100.

24 P. Ehrenfreund, M. P. Bernstein, J. P, Dworkin, S. A. Sandford, and L. J. Allamandola, *Astrophys. J.* 2001, 550, L95.

25 M. P. Bernstein, S. F. M. Ashbourn, S. A. Sandford, and L. J. Allamamdola, *Astrophys. J.* 2004, **601**, 365.

26 I. L. ten Kate, J. R. C. Garry, Z. Peeters, R. Qinn, B. Foing, and P. Ehrenfreund, *Meteor. Planet. Sci.* 2005, **40**, 1185.

27 G. E. Orzechowska, J. D. Goguen, P. V. Johnson, A. Tsapin, and I. Kanik, *Icarus*, 2007, **187,** 584.

28 A. M. Ferreira-Rodrigues, M. G. P. Homem, A. Naves de Brito, C. R. Ponciano, and E. F. da Silveira, *Int. J. Mass Spectrom.* 2011, **306**, 77.

29 P. V. Johnson, R. Hodyss, V. F. Chernow, D. M. Lipscomb, and J. D. Goguen, *Icarus*, 2012, **221**, 800.

30 E. Sagstuen, A. Sanderud, and E. O. Hole, *Rad. Research*, 2004, **162**, 112

31 R. I. Kaiser and K. Roessler, *Astrophys J.*, 1997, **475**, 144.

32 I. L. Barnett, A. Lognell, and M. S. Gudipati, *Astrophys. J.* 2013, **743**. 13

33 P.D. Holtom, Ch. Bennett, Y. Osamura, N. J. Mason, and R. I. Kaiser, *Astrophys. J.* 2005, **626**, 940.

34 A. Lafosse, M. Bertin and R. Ariza, *Progr. Surf. Sci.*, **84**, 177.

35 R. I. Kaiser, A. M. Stockton, Y. S. Kim, E. C. Jensen, and AR. A. Mathies, *Astrophys. J.* 2013, **756**, 111.

36 F. J. Gordillo-Vázquez, V. J. Herrero, and I. Tanarro, *Chem. Vap. Deposition*, 2007, **13**, 267

37 F.L. Tabarés, D. Tafalla, I. Tanarro, V. J. Herrero and A. M. Islyaikin, *Vacuum*, 2004, **73**, 161.

38 I. Tanarro, J. A. Ferreira, V. J. Herrero, F.L. Tabarés, C. Gómez-Aleixandre. *J. Nucl. Mat.*, 2009, **390-391**, 696.

39 M. Bauer, T. Schwarz-Selinger, W. Jacob, A. von Keudell, *J. Appl. Phys.* 2005, 98, 073302.

40 D. P. Liu, I. T. Martin, J. Zhou, E. R. Fisher, E R, *Pure Appl. Chem*., 2006 , 78, : 1187.

41 M. Mozetic, A. Vesel, D. Alegre, F.L. Tabares, J. Appl. Phys., 2011, **110**, 053302-10.

42 I. Tanarro, V. J. Herrero, A. M. Islyaikin, I. Méndez, F. L. Tabarés, D. Tafalla, *J. Phys. Chem. A*, 2007, **111**, 9003.

43 B. Maté, A. Medialdea, M. A. Moreno, R. Escribano and V. J. Herrero, *J. Phys. Chem. B*, 2003, **107**, 11098.

44 Y.Rodríguez Lazcano, B. Maté, O. Gálvez, V. J. Herrero, I. Tanarro and R. Escribano, *J. Quant. Spectr. Rad. Transf*., 2012**, 113,** 1266.

45 D. Drouin et al., 2011, Monte Carlo Simulation of Electron Trajectory in Solids (CASINO version 2.48) Université de Sherbrooke, Sherbrooke, Quebec, Canada., www.gel.usherbrooke.ca/casino

46 M. J. Loeffler, G. A. Baratta, M. E. Palumbo, G. Strazzulla and R. A. Baragiola, *Astron. Astrophys* 2005, **435**, 587.

47 O. Gálvez, I.K. Ortega, B. Maté, B. Martín-Llorente, V.J. Herrero, R. Escribano, P.J. Gutierrez, *Astron. Astrophys*., 2007, 472, 691.

48 S. Jheeta, S. Ptasinka, B. Sivaraman, and N. J. Mason, *Chem. Phys. Lett.* 2012, **543**, 208.

49 J. B. Bossa, F. Borget, F. Duvernay, P. Theulé, and T, Chiavassa, *J. Phys. Chem. A.*, 2008, **112**, 5113.

50 O. Poch, A. Noblet, F. Stalport, J. J,. Correia, N. Grand, G. Szopa, and P. Coll, *Planet. Space. Sci.* 2013, **85**, 188